nature geoscience

ARTICLES

https://doi.org/10.1038/s41561-018-0204-7

Lower land-use emissions responsible for increased net land carbon sink during the slow warming period

Shilong Piao[1,2,3*], Mengtian Huang[3], Zhuo Liu[3], Xuhui Wang[3,4], Philippe Ciais[4], Josep G. Canadell[5], Kai Wang[3], Ana Bastos[4], Pierre Friedlingstein[6], Richard A. Houghton[7], Corinne Le Quéré[8], Yongwen Liu[1,2,3], Ranga B. Myneni[9], Shushi Peng[3], Julia Pongratz[10,11], Stephen Sitch[12], Tao Yan[3], Yilong Wang[4], Zaichun Zhu[3], Donghai Wu[3] and Tao Wang[1,2]

The terrestrial carbon sink accelerated during 1998–2012, concurrently with the slow warming period, but the mechanisms behind this acceleration are unclear. Here we analyse recent changes in the net land carbon sink (NLS) and its driving factors, using atmospheric inversions and terrestrial carbon models. We show that the linear trend of NLS during 1998–2012 is about 0.17 ± 0.05 Pg C yr^{-2}, which is three times larger than during 1980–1998 (0.05 ± 0.05 Pg C yr^{-2}). According to terrestrial carbon model simulations, the intensification of the NLS cannot be explained by CO_2 fertilization or climate change alone. We therefore use a bookkeeping model to explore the contribution of changes in land-use emissions and find that decreasing land-use emissions are the dominant cause of the intensification of the NLS during the slow warming period. This reduction of land-use emissions is due to both decreased tropical forest area loss and increased afforestation in northern temperate regions. The estimate based on atmospheric inversions shows consistently reduced land-use emissions, whereas another bookkeeping model did not reproduce such changes, probably owing to missing the signal of reduced tropical deforestation. These results highlight the importance of better constraining emissions from land-use change to understand recent trends in land carbon sinks.

Concurrent with the warming hiatus of 1998–2012[1–3], the vegetation greening trend observed from several satellite products stalled after 1998 in most regions[4–8] while the global land carbon sink has continued to increase[9,10]. Keenan et al.[9] and Ballantyne et al.[10] analysed this signal from the residual land carbon sink calculated by difference between emissions from fossil fuel and land use, ocean uptake and atmospheric CO_2 growth rate. The mechanisms behind the recent increase in residual land carbon sink were not the same in the two studies. Keenan et al.[9] suggest both increasing photosynthesis and decreased respiration, whereas Ballantyne et al.[10] suggest that decreasing photosynthesis and thus reduced respiration is the only mechanism through which the residual land carbon sink increased during the hiatus. Furthermore, the seasonal and spatial patterns of changes in the land carbon sink do not match those of temperature changes[11]. We note that systematic errors in land-use emissions[12] directly transfer as a bias of the residual land carbon sink[13,14]. Thus, instead of the residual land carbon sink, we revisit changes in the NLS, including land-use emission and its driving factors, using atmospheric inversions and land carbon models.

The NLS estimated from the two inversions (see Methods) and from the global CO_2 budget[15] show a three-times-faster increase after 1998 (0.17 ± 0.05 Pg C yr^{-2}, mean $\pm$ 1 standard error) than in the decades before (0.05 ± 0.05 Pg C yr^{-2}) (Fig. 1 and Supplementary Table 1, see Methods). The year 1998 is used as the beginning of the warming hiatus by the Intergovernmental Panel on Climate Change (IPCC)[16] and the previous carbon cycle study[17], but using 2001 or 2002 as the starting year of the warming hiatus yields similar results (Supplementary Table 2). The increasing positive trend in NLS after 1998 (NLS intensification) is also found on a 5-year moving window (Supplementary Fig. 1) and in different inversion versions with more atmospheric CO_2 measurement sites but for shorter periods (Supplementary Table 3 and Fig. 2).

NLS can be decomposed as the sum of three components, net primary productivity (NPP), heterotrophic respiration and fires in natural ecosystems (HR + F) and net carbon emissions from land-use change (E_{LUC}). The fraction of fire emissions that happens during land-use change, known as deforestation fires, is included in E_{LUC}, whereas carbon emission from fossil fuels for land management is not included in E_{LUC}. To explain why NLS increased faster after 1998, we consider three mechanisms: (M1) NPP increased faster than before, forcing a sink intensification; (M2) HR + F increased at a slower rate than before or declined, consistent with slower warming rates; and (M3) E_{LUC} emissions decreased[18].

[1]Key Laboratory of Alpine Ecology and Biodiversity, Institute of Tibetan Plateau Research, Chinese Academy of Sciences, Beijing, China. [2]Center for Excellence in Tibetan Earth Science, Chinese Academy of Sciences, Beijing, China. [3]Sino-French Institute for Earth System Science, College of Urban and Environmental Sciences, Peking University, Beijing, China. [4]Laboratoire des Sciences du Climat et de l'Environnement, CEA CNRS UVSQ, Gif-sur-Yvette, France. [5]Global Carbon Project, CSIRO Oceans and Atmosphere, Canberra, Australian Capital Territory, Australia. [6]College of Engineering, Mathematics and Physical Sciences, University of Exeter, Exeter, UK. [7]Woods Hole Research Center, Falmouth, MA, USA. [8]Tyndall Centre for Climate Change Research, University of East Anglia, Norwich Research Park, Norwich, UK. [9]Department of Earth and Environment, Boston University, Boston, MA, USA. [10]Max Planck Institute for Meteorology, Hamburg, Germany. [11]Ludwig-Maximilians-Universität München, Department of Geography, Munich, Germany. [12]College of Life and Environmental Sciences, University of Exeter, Exeter, UK. *e-mail: slpiao@pku.edu.cn

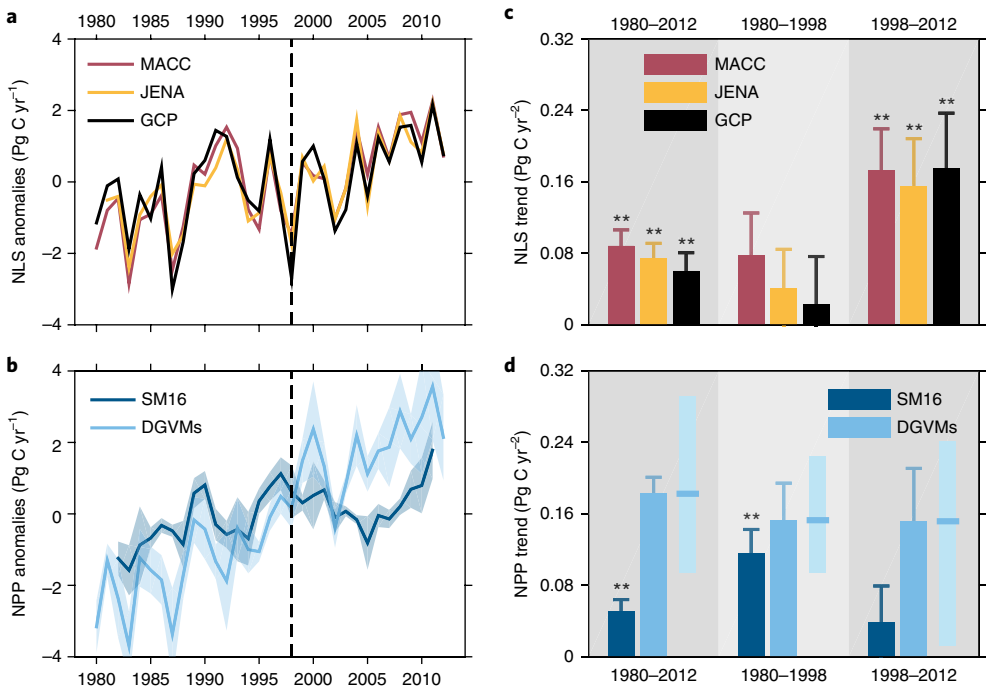

Fig. 1 | Anomalies and linear trends of global annual NLS and NPP. Trends were estimated for three time periods: 1980–2012, 1980–1998 and 1998–2012. Top panels show NLS. Bottom panels show NPP. In the left panels (**a** and **b**), a positive value refers to a net carbon sink. The shaded areas in **b** indicate data uncertainty (±1σ). In the right panels (**c** and **d**), we denote significant trends ($P<0.05$) with two asterisks. The error bars in the right panels indicate the standard error of linear trend. In **d**, the range of the data (minimum to maximum) across different models is given as coloured vertical bars with the solid line showing the average value. Different colours correspond to different sources of data (see also Methods).

Trends in NPP

For the first mechanism, we analysed NPP changes over the past 30 years using the dynamic global vegetation models (DGVMs) from the TRENDY project and satellite-observation-based NPP from Smith et al.[4] (hereafter SM16, see Methods). As shown in Fig. 1b and d, both satellite-derived NPP and modelled NPP showed significant positive trends (an indication of enhanced carbon assimilation) before 1998 (SM16: 0.12 ± 0.03 Pg C yr^{-2}, $P<0.01$; mean of DGVMs: 0.15 ± 0.04 Pg C yr^{-2}, $P<0.01$). After 1998, however, the satellite-based NPP shows a significantly ($P<0.05$) smaller positive trend (0.04 ± 0.04 Pg C yr^{-2}, $P>0.05$) than before. By comparison, four of the eight DGVMs do not show deceleration of NPP (a reduced trend of NPP) after 1998, with the trend change of NPP ranging from -0.08 ± 0.05 Pg C yr^{-2} ($P<0.05$) to 0.11 ± 0.06 Pg C yr^{-2} ($P<0.01$) (Supplementary Fig. 3). On average, the DGVMs show almost no change in the NPP trend (-0.001 ± 0.067 Pg C yr^{-2}, $P>0.1$) between the period before 1998 and that after 1998 (Fig. 2), and can thus explain very little (<1%) of the intensification of NLS after 1998. A recent commentary[19] suggested that the disagreement of NPP trends between SM16 and DGVM is probably due to the underestimate of the CO_2 fertilization effect on satellite-based NPP. However, a continued increase of CO_2 concentration over the past three decades may not explain the intensification of NLS after 1998. The leaf area index derived from GIMMS satellite products stalled in the recent period 1998–2012, which is not captured by DGVMs (Supplementary Fig. 4). This overestimate of the leaf area index trend in the period after 1998 suggests that DGVMs may underestimate the deceleration of NPP during 1998–2012 captured in SM16. Therefore, the forcing from NPP change alone cannot explain why NLS intensified.

Trends in HR + F

To analyse the second mechanism (M2), we analysed changes in HR based on the same DGVM results[13,20]. As shown in Fig. 2 and

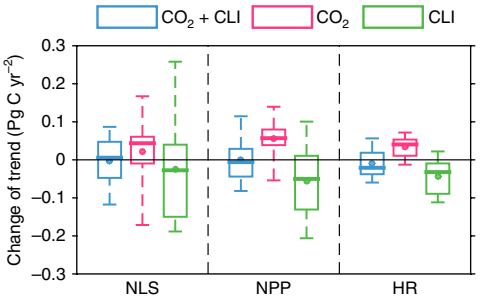

Fig. 2 | Change in the trend of NLS, NPP and HR between 1998–2012 and 1980–1998 estimated by DGVMs. For each model, the changes in the trend of NLS/NPP/HR were obtained as the trend of each variable during 1998–2012 minus that during 1980–1998. Results for the effect of rising atmospheric CO_2 concentration (CO_2), climate change (CLI), and the above two factors combined (CO_2 + CLI) are shown. On each box, the central line marks the median, the edges of the box correspond to the 25th and 75th percentiles, and the whiskers extend to the range of the data. The solid dot shows the average value of the model results.

Supplementary Table 1, a reduction in the positive trend of HR (a deceleration of carbon emission from HR) in simulations where models were driven by changing CO_2 and climate was found by most DGVMs, with six out of the eight models showing a reduced trend of HR after 1998 ranging from -0.06 ± 0.03 Pg C yr^{-2} ($P<0.01$) to 0.06 ± 0.08 Pg C yr^{-2} ($P>0.05$). The small deceleration of HR (-0.01 ± 0.04 Pg C yr^{-2}, $P>0.05$), however, accounts for less than 9% (−47% to 49%) of the observed intensification of NLS. According to factorial DGVM simulations, the effect of climate change alone (see Methods) did cause a significant deceleration

of HR in the period 1998–2012 (-0.04 ± 0.05 Pg C yr^{-1}, $P > 0.05$) compared to the period 1980–1998 (Fig. 2), consistent with a slower warming rate between 1998 and 2012. However, the climate-driven HR deceleration (deceleration in carbon emission) is also paralleled by a NPP deceleration (deceleration in carbon uptake) due to climate change alone in the DGVMs (-0.06 ± 0.10 Pg C yr^{-2}, $P > 0.05$; Fig. 2). This indicates that the NLS intensification during 1998–2012 cannot be attributed to climate change alone in the DGVMs. The simulation results of these models further show that rising atmospheric CO_2 can only explain 19% of the NLS intensification (Fig. 2), and that the combinations of CO_2 and climate change cancel each other. These results suggest that mechanisms other than CO_2 fertilization and climate change are responsible for the observed intensification of the NLS.

Besides HR, a reduction in natural fire emission could also be a cause of the intensification in the NLS. Accounting for natural fires at the global scale remains challenging, because satellite-based burn area observations cannot readily distinguish natural fires from other causes[21,22]. Therefore, we analysed trends in fire simulated by four TRENDYv2 DGVMs, which considered wild-fire processes. The models exhibited large differences in the change of fire emissions trend during the two periods (CLM4.5: -0.052 ± 0.020 Pg C yr^{-1}, $P < 0.01$; LPJ: 0.004 ± 0.009 Pg C yr^{-1}, $P > 0.05$; VISIT: 0.007 ± 0.018 Pg C yr^{-1}, $P > 0.05$; LPJ-GUESS: 0.013 ± 0.024 Pg C yr^{-1}, $P > 0.05$) (Supplementary Fig. 5). However, even considering the full model range of trend change estimates, the natural fire emission probably contributes negatively to NLS intensification ($-6\% \pm 25\%$).

Trends in E_{LUC}

Over the past thirty years, there has been a slow-down of forest losses[23–27]. According to the latest Forest Resources Assessment (FRA) by the Food and Agriculture Organization (FAO) of the United Nations[28], the annual rate of net forest loss decreased from 7.27 M ha yr^{-1} in the 1990s to 3.99 M ha yr^{-1} in the 2000s, primarily owing to less logging in tropical regions and increased plantations in northern temperate lands (Supplementary Table 4 and Fig. 6). Therefore, the NLS intensification can also reflect decreased E_{LUC} during 1998–2012.

We estimated E_{LUC} using the latest version of the bookkeeping model from Houghton et al.[12] (hereafter BK), which was widely used and adopted by the Global Carbon Project in developing annual global carbon budget[29]. The global E_{LUC} is a source of 1.13 Pg C yr^{-1}, which is found mostly in tropical regions (1.31 Pg C yr^{-1}), primarily southeast Asia (0.54 Pg C yr^{-1}), South America (0.38 Pg C yr^{-1}) and Africa (0.38 Pg C yr^{-1}) (Supplementary Fig. 7a). Tropical regions are found to be the largest contributor to global E_{LUC} emissions, followed by the Southern Hemisphere temperate regions as a slight source (1% of global E_{LUC}) (Supplementary Fig. 7a). We then compared the linear trend of E_{LUC} over the globe between 1980–1998 and 1998–2012. The deceleration of E_{LUC} contributes to a trend change of 0.09 ± 0.01 PgC yr^{-2} ($P < 0.01$) (Fig. 3), explaining 73% of NLS intensification. This result suggests that the faster increase of NLS after 1998 is primarily explained by decreasing E_{LUC}.

As shown in Fig. 3, the deceleration in global E_{LUC} between 1980–1998 and 1998–2012 is attributed to tropical regions, where a decline of -0.08 ± 0.01 Pg C yr^{-2} ($P < 0.01$) in E_{LUC} trend is found (about 92% of the total decrease in the global E_{LUC} trend). The decline was largely in southeast Asia (-0.05 ± 0.01 Pg C yr^{-2}, $P < 0.01$) and South America (-0.016 ± 0.004 Pg C yr^{-2}, $P < 0.01$) (Fig. 3), where the annual rate of net forest loss declined during the 2000s compared with the 1990s[28]. For example, the rate of net forest loss in South America decreased from 4 M ha yr^{-1} during the 1990s to 3.87 M ha yr^{-1} during the 2000s, whereas the net loss rate in southeast Asia during the 2000s (0.64 M ha yr^{-1}) was only 30% of that during the 1990s (2.11 M ha yr^{-1}) (Supplementary Fig. 6 and Table 4). For Northern Hemisphere temperate regions, E_{LUC} was found to decelerate between the two periods, with a linear trend of -0.010 ± 0.001 Pg C yr^{-2} after 1998 ($P < 0.01$; about 11% of the total decrease in global E_{LUC} trend). Temperate North America accounted for the largest fraction (89%; -0.009 ± 0.006 Pg C yr^{-2}, $P < 0.01$) of decreasing E_{LUC} in the northern temperate zone, mainly because the forest area decrease of -0.35 M ha yr^{-1} in the 1990s was reversed to an increase of 0.22 M ha yr^{-1} after 2000[28] (Supplementary Fig. 6 and Table 4).

In addition to BK, based on the FAO/FRA land-use areas and regional carbon response curves to land-use change[14], we also explored E_{LUC} estimates using two other methods, which are: (1) the bookkeeping model of Hansis et al.[30] (hereafter BKH) based on Land Use Harmonization data from 1500 to 2004[31] and the Global Carbon Project update from 2005 to 2012[13] (see Methods), and (2) E_{LUC} estimated from the difference between the net land–atmosphere CO_2 flux from atmospheric inversions and the fraction of this flux attributed to natural ecosystems simulated under the TRENDY S2 DGVM simulation (hereafter E_{ILD}; see Methods). Globally, the change in trend of global E_{LUC} after 1998 by E_{ILD} (-0.07 ± 0.05 Pg C yr^{-2}, $P < 0.05$) was similar to that by BK, but BKH estimated little change in the trend of E_{LUC} (-0.01 ± 0.01 Pg C yr^{-2}, $P > 0.05$) for the same period. This lack of trend change by BKH may come from uncertainties in the land cover input dataset. Important differences between the land-use input used in BK, which is directly based on FAO/FRA, and the harmonized land-use dataset by Hurtt et al.[31] used in BKH are the assumptions on shifting cultivation in the tropics and additional assumptions introduced in the latter dataset to make the country-level FAO/FRA data spatially explicit. Forest cover changes are not explicitly indicated by the harmonized land-use dataset but are deduced from changes in agricultural areas and thus can differ greatly from forest inventory data both in magnitudes and in trends (Supplementary Fig. 8). For example, the BKH-estimated E_{LUC} over South America exhibited positive change (0.007 ± 0.008 Pg C yr^{-2}, $P > 0.05$) during the warming hiatus period, which is in contrast to forest survey data suggesting a reduced rate of deforestation in the 2000s[28]. The shift of land cover dataset in 2004 is also a potential issue, making BKH more uncertain in estimating change in the E_{LUC} trend during the most recent decade. The general consensus between BK and E_{ILD} in estimating the change in the E_{LUC} trend globally and over South America suggests the potential of utilizing this new method in estimating E_{LUC}. However, it also differs from BK in estimating the change in the trend of E_{LUC} at the regional scale, for example, over Africa (-0.002 ± 0.001 Pg C yr^{-2}, $P < 0.05$ by BK versus 0.04 ± 0.03 Pg C yr^{-2}, $P < 0.05$ by E_{ILD}; Supplementary Fig. 7b). The lack of atmospheric CO_2 observations over Africa can be a large source of uncertainties in atmospheric inversion, as indicated by the large error bars in regional E_{LUC} estimates (Supplementary Fig. 7b). The uncertainties in land carbon models[20] are also propagated in E_{ILD}.

In summary, our results confirm an intensification in NLS during the warming hiatus (1998–2012) as compared to the preceding period (1980–1998). Using different approaches, we found that a number of drivers were responsible for the enhanced rate of the NLS. The decreasing trend in net carbon emissions from land-use change was the dominant cause during the warming hiatus period. The decreasing emissions from land-use change were not driven by a lower rate of warming during this period, but by reduced deforestation in the tropics and increased afforestation in Northern Hemisphere temperate regions. Consistent with Keenan et al.[9], we found a lower positive trend of HR owing to a lower rate of warming during the second period. But unlike theirs, our analysis, based on an ensemble of DGVMs under different scenarios instead of a semi-empirical model[9], shows little effect of HR trends on the NLS, mainly because of the compensating effects of CO_2 fertilization (increasing carbon emissions from HR through higher input) and

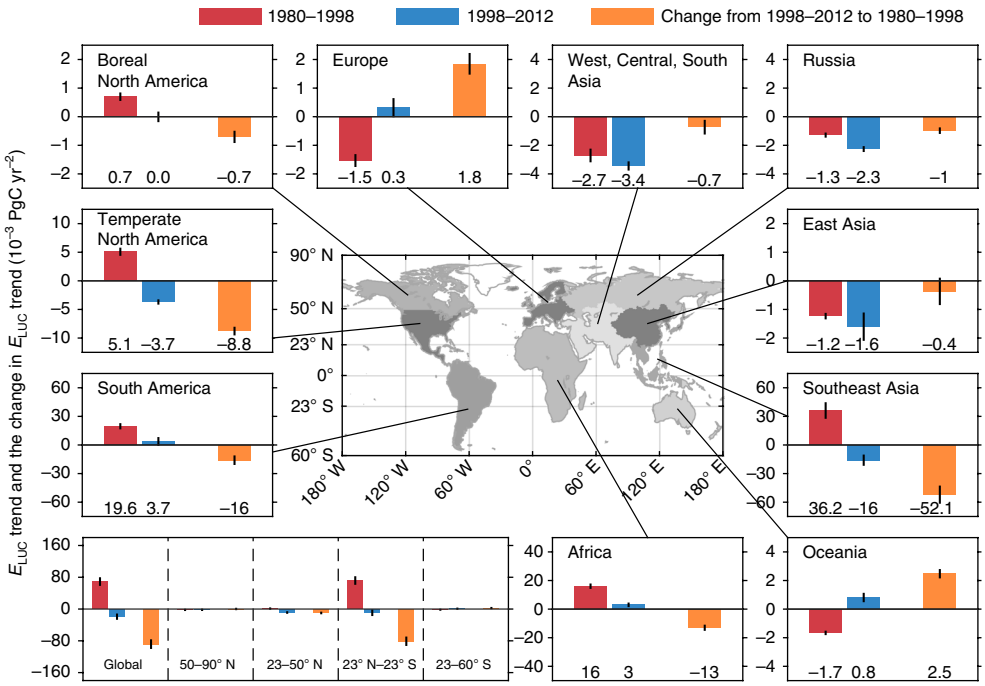

Fig. 3 | Linear trend of E_{LUC} and change in E_{LUC} trend between 1998–2012 and 1980–1998. The bottom left panel shows results at the latitudinal scale, including the boreal (50° N–90° N), northern temperate (23° N–50° N), tropical (23° N–23° S) and southern temperate (23° S–60° S) regions. The E_{LUC} trends during each of the two periods as well as the change in the E_{LUC} trend between two periods are determined from annual E_{LUC} values obtained using the bookkeeping method. A positive trend refers to increased E_{LUC} during the corresponding period, whereas a negative trend refers to decreased E_{LUC} during the corresponding period. The error bars indicate the uncertainty for the E_{LUC} trend or the change in E_{LUC} trend. The uncertainty of the linear trend was estimated as the standard error of the linear regression coefficient (slope), while the uncertainty of the change in the E_{LUC} trend was estimated using bootstrap analyses.

climate change (decreasing carbon emissions from HR). We note that large uncertainties still remain with estimates of carbon flux from land-use change and its trend over the last thirty years, particularly in East Asia, South America, Africa and Europe. Reducing this uncertainty is a top priority for future work to enable more accurate predictions of the future evolution of the global carbon cycle and its feedback to climate change. To this end, detailed information on LULCC transitions[25,32] with high spatio-temporal resolution, and on carbon response functions to these transitions[27,33] is needed. In addition, various forms of land-use management (such as wood harvest, shifting cultivation, cropland management, fire management, peatland drainage) are often inconsistently and incompletely represented in DGVMs[13,14]. A better characterization of these critical processes is required for future studies.

Methods

Methods, including statements of data availability and any associated accession codes and references, are available at https://doi.org/10.1038/s41561-018-0204-7.

Received: 9 August 2017; Accepted: 11 July 2018;
Published online: 20 August 2018

References

1. Easterling, D. R. & Wehner, M. F. Is the climate warming or cooling? *Geophys. Res. Lett.* **36**, L08706 (2009).
2. Kaufmann, R. K., Kauppi, H., Mann, M. L. & Stock, J. H. Reconciling anthropogenic climate change with observed temperature 1998-2008. *Proc. Natl. Acad. Sci. USA* **108**, 11790–11793 (2011).
3. Cohen, J. L., Furtado, J. C., Barlow, M. & Alexeev, V. A. Asymmetric seasonal temperature trends. *Geophys. Res. Lett.* **39**, L04705 (2012).
4. Smith, W. K. et al. Large divergence of satellite and Earth system model estimates of global terrestrial CO_2 fertilization. *Nat. Clim. Change* **6**, 306–310 (2016).
5. Zhao, M. & Running, S. W. Drought-induced reduction in global terrestrial net primary production from 2000 through 2009. *Science* **329**, 940–943 (2010).
6. Jong, R., Verbesselt, J., Schaepman, M. E. & Bruin, S. Trend changes in global greening and browning: contribution of short-term trends to longer-term change. *Glob. Change Biol.* **18**, 642–655 (2012).
7. Mohammat, A. et al. Drought and spring cooling induced recent decrease in vegetation growth in InnerAsia. *Agric. For. Meteorol.* **178**, 21–30 (2013).
8. Kong, D., Zhang, Q., Singh, V. P. & Shi, P. Seasonal vegetation response to climate change in the Northern Hemisphere (1982–2013). *Glob. Planet. Change* **148**, 1–8 (2017).
9. Keenan, T. F. et al. Recent pause in the growth rate of atmospheric CO_2 due to enhanced terrestrial carbon uptake. *Nat. Commun.* **7**, 13428 (2016).
10. Ballantyne, A. et al. Accelerating net terrestrial carbon uptake during the warming hiatus due to reduced respiration. *Nat. Clim. Change* **7**, 148–152 (2017).
11. Zhu, Z. et al. The accelerating land carbon uptake of the 2000s may not be driven predominantly by the warming hiatus. *Geophys Res Lett.* **45**, 1402–1409 (2018).
12. Houghton, R. A. & Nassikas, A. A. Global and regional fluxes of carbon from land use and land cover change 1850-2015. *Glob. Biogeochem. Cycles* **31**, 456–472 (2017).
13. Le Quéré, C. et al. Global carbon budget 2013. *Earth Syst. Sci. Data* **6**, 235–263 (2014).
14. Houghton, R. A. et al. Carbon emissions from land use and land-cover change. *Biogeosciences* **9**, 5125–5142 (2012).
15. Le Quéré, C. et al. Global carbon budget 2015. *Earth Syst. Sci. Data* **7**, 349–396 (2015).
16. Hartmann, D. L. et al. in *Climate Change 2013: The Physical Science Basis* (eds Stocker, T. F. et al.)192–194 (Cambridge Univ. Press, Cambridge, 2013).
17. Ballantyne, A. et al. Accelerating net terrestrial carbon uptake during the warming hiatus due to reduced respiration. *Nat. Clim. Change* **7**, 148–152 (2017).
18. Grassi, G. et al. The key role of forests in meeting climate targets requires science for credible mitigation. *Nat. Clim. Change* **7**, 220–226 (2017).
19. De Kauwe, M. G. et al. Satellite based estimates underestimate the effect of CO_2 fertilization on net primary productivity. *Nat. Clim. Change* **6**, 892–893 (2016).

20. Sitch, S. et al. Recent trends and drivers of regional sources and sinks of carbon dioxide. *Biogeosciences* **12**, 653–679 (2015).
21. Giglio, L., Randerson, J. T. & van der Werf, G. R. Analysis of daily, monthly, and annual burned area using the fourth-generation global fire emissions database (GFED4). *J. Geophys. Res. Biogeosci.* **118**, 317–328 (2013).
22. Andela, N. et al. A human-driven decline in global burned area. *Science* **356**, 1356–1362 (2017).
23. Rudel, T. K. et al. Forest transitions: towards a global understanding of land use change. *Glob. Environ. Change* **15**, 23–31 (2005).
24. Sánchezcuervo, A. M., Aide, T. M., Clark, M. L. & Etter, A. Land cover change in Colombia: surprising forest recovery trends between 2001 and 2010. *PLoS ONE 7* e43943 (2012)..
25. Magliocca, N. R. et al. Synthesis in land change science: methodological patterns, challenges, and guidelines. *Reg. Environ. Change* **15**, 211–226 (2015).
26. Chazdon, R. L. et al. Carbon sequestration potential of second-growth forest regeneration in the Latin American tropics. *Sci. Adv.* **2**, e1501639 (2016).
27. Poorter, L. et al. Biomass resilience of neotropical secondary forests. *Nature* **530**, 211 (2016).
28. *Global Forest Resources Assessment 2015: How are the world's forests changing?* (FAO, 2015); http://www.fao.org/forest-resources-assessment/en/
29. Le Quéré, C. et al. Global carbon budget 2014. *Earth Syst. Sci. Data* **7**, 47–85 (2015).
30. Hansis, E., Davis, S. J. & Pongratz, J. Relevance of methodological choices for accounting of land use change carbon fluxes. *Glob. Biogeochem. Cycles* **29**, 1230–1246 (2015).
31. Hurtt, G. C. et al. Harmonization of land-use scenarios for the period 1500-2100: 600 years of global gridded annual land-use transitions, wood harvest, and resulting secondary lands. *Clim. Change* **109**, 117–161 (2011).
32. Erb, K. H. et al. Bias in the attribution of forest carbon sinks. *Nat. Clim. Change* **3**, 854–856 (2013).
33. Poeplau, C. et al. Temporal dynamics of soil organic carbon after land-use change in the temperate zone—carbon response functions as a model approach. *Glob. Change Biol.* **17**, 2415–2427 (2011).

Acknowledgements

This study was supported by the Strategic Priority Research Program (A) of the Chinese Academy of Sciences (grant XDA20050101), the International Partnership Program of Chinese Academy of Sciences (grant 131C11KYSB20160061), the National Natural Science Foundation of China (41530528), and the 111 Project (B14001). We thank the TRENDY modelling group for providing the model simulation data.

Author contributions

S. Piao designed the study. M.H. and Z.L performed the analysis. S. Piao and Z.L drafted the paper. All authors contributed to the interpretation of the results and to the text.

Competing interests

The authors declare no competing interests.

Additional information

Supplementary information is available for this paper at https://doi.org/10.1038/s41561-018-0204-7.

Reprints and permissions information is available at www.nature.com/reprints.

Correspondence and requests for materials should be addressed to S.P.

Publisher's note: Springer Nature remains neutral with regard to jurisdictional claims in published maps and institutional affiliations.

Methods

Satellite-based NDVI and NPP data. The Normalized Difference Vegetation Index (NDVI), which has been widely used to monitor vegetation activity, was obtained from the Global Inventory Modelling and Mapping Studies (GIMMS) third-generation product ($NDVI_{3g}$) at a resolution of 8 km × 8 km from 1982 to 2015[34].

The satellite-derived NPP was from MODIS[5] and a recent study by Smith et al.[4] (SM16). For the latter, NPP was calculated based on the MODIS NPP algorithm[5], but driven by the 30-year (1982–2011) GIMMS fraction of photosynthetically active radiation and leaf area index data[4]. Further details about satellite-derived NPP data can be found in refs. [4] and [5]. We note that the MODIS results only cover the period from 2001 onwards. Therefore, we included the MODIS results only in Supplementary Fig. 9 to show that the stall of NPP during the warming hiatus period is not an artefact from the single long-term satellite-derived NPP dataset from Smith et al.[4].

DGVMs. An ensemble of eight DGVMs (see Supplementary Table 5), taken from the project "Trends and drivers of the regional scale sources and sinks of carbon dioxide" (TRENDY) were used to simulate the carbon balance of terrestrial ecosystems during the period 1980–2012. These models provided outputs of net biome productivity (NBP), NPP and HR. Here we used NBP to reflect the magnitude of NLS (NLS = NBP = NPP − HR − D, where D refers to other losses of carbon due to disturbance, including carbon emissions from land-use change). We adopted the convention that a sink of CO_2 is defined as positive (removing CO_2 from the atmosphere).

The DGVMs were coordinated to perform three simulations (S1, S2 and S3) following the TRENDY protocol[20]. In simulation S1, only atmospheric CO_2 concentration was varied. In simulation S2, atmospheric CO_2 and climate were varied. In simulation S3, atmospheric CO_2, climate and land use were varied. The effects of rising atmospheric CO_2, climate change and land-use change on NLS can then be obtained from S1, the difference between S2 and S1, and the difference between S3 and S2, respectively. All models used the same forcing datasets, of which global atmospheric CO_2 concentration was from the combination of ice-core records and atmospheric observations[35]; historical climate fields were from the CRU-NCEP dataset (ftp://ftp.cdc.noaa.gov/); land-use data were from the Land Use Harmonization dataset[31] based on the History Database of the Global Environment (HYDE)[36]. All the model outputs were resampled to a spatial resolution of 0.5° × 0.5°based on the nearest-neighbour method.

Note that there is a large difference between TRENDYv2 and TRENDYv4 in their estimates of the NLS trend before and after 1998 under the S3 simulation (Supplementary Fig. 10). On average, NLS in TRENDYv2 shows a non-significant trend before 1998 and a significant increasing trend after 1998 (Supplementary Fig. 10h), which is consistent with the results from the global carbon budget and atmospheric inversions. However, in TRENDYv4, an opposite case was found (Supplementary Fig. 10h). This difference between TRENDYv2 and TRENDyv4 in simulating the observed NLS trend mainly results from the simulation of land-use change rather than from S2 simulation (Supplementary Fig. 10h). This not only indicates large uncertainties in the simulation of land-use change (Supplementary Fig. 7), but suggests the potential effect of land-use change on the NLS trend. Although TRENDYv4 used an updated and improved input of land-use change maps (HYDE3.2)[37] compared with TRENDYv2 (HYDE3.1), we did not adopt it to estimate carbon emissions from land-use change given that it did not capture the trend of NLS before and after 1998. Overall, we only used TRENDY results derived from the S1 and S2 simulations in our main text, and propose a way to estimate land-use change emission by combining the results from atmospheric inversions and TRENDY models under the S2 simulation (see below).

Global carbon budget. To gain a better understanding of the NLS, we also used data from the global carbon budget coordinated by the Global Carbon Project[15]. Here the net land sink was inferred as a residual of fossil fuel emissions, atmospheric CO_2 accumulation and ocean sink, which is independent from atmospheric inversions.

Atmospheric CO_2 inversion data. Atmospheric CO_2 inversions offer a method in which CO_2 observation networks, transport models and a prior knowledge of fluxes are utilized to estimate net land-atmosphere carbon exchange[38]. This top-down approach allows us to compare the magnitude of the NLS with that from the bottom-up method based on DGVMs. Given our long-term study period from 1980 to 2012, here we used two inversion products: MACC_v15 from Chevallier et al.[39] (hereafter MACC, available time period: 1979–2015) and JENA_S81_v3.8 from Rödenbeck et al.[40] (hereafter JENA, available time period: 1981–2014). The original spatial resolution of MACC and JENA is 1.875° latitude × 3.75° longitude and 3.75° latitude × 5° longitude, respectively.

It should be noted that there are differences between these two inversions in number of observation sites as constraint, transport models and prior flux information[38]. As recommended in previous studies[38,41], a standard fossil fuel and cement production flux should be subtracted from the total posterior fluxes when comparing net land flux from different CO_2 inversions. This is because differences in prior fossil fuel and cement production flux will manifest as differences in the estimated natural flux[36]. Thus, here we took the fossil fuel flux that is used in the Global Carbon Project carbon budget as a standard and subtracted it from the total posterior fluxes for both CO_2 inversions to obtain the 'fossil-fuel-corrected' NLS, although the global fossil fuel emissions are quite consistent between the two inversions and with the Global Carbon Project data (Supplementary Fig. 11). We note that the fossil fuel and cement production flux data used in the Global Carbon Project carbon budget was from the Carbon Dioxide Information Analysis Center (http://cdiac.ornl.gov/trends/emis/meth_reg.html) and energy statistics published by BP (https://www.bp.com/en/global/corporate/what-we-do/bp-at-a-glance.html).

E_{LUC}. We explored E_{LUC} estimates using three different approaches. First, we used the estimates by Houghton et al.[12] (BK) for carbon fluxes due to land-use change. In this method, ground-based measurements of carbon density are combined with land cover change data from the FRA/FAO using a semi-empirical bookkeeping model, in which standard growth and decomposition curves are used to track changes in carbon pools[14]. Using the estimate by Houghton et al.[12] is consistent with the global carbon budget estimates provided by the Global Carbon Project[42], but may conceal large uncertainties associated with land-use change itself as well as related carbon fluxes. We therefore include in the Supplementary Information two additional approaches. The second approach to estimate E_{LUC} in this study is also a bookkeeping method but from Hansis et al.[30] (BKH). Although BKH largely follows the bookkeeping method developed by Houghton et al.[43,44] (BK), there are key differences between BKH and BK: BKH is spatially explicit at a resolution of 0.5° × 0.5°[30], whereas BK is constructed based on aggregated, non-spatial national and international statistics[14]; BKH used the Land Use Harmonization dataset from 1500 to 2004[28] and the Global Carbon Project update from 2005 to 2012 as input[30] while BK used FAO/FRA land use change data[14]; other differences between BKH and BK are the accounting of successive land use and land cover change (LULCC) events including their interactions in BKH and different assumptions on the allocation of agricultural land on natural vegetation[30]. Note that the data available now from Houghton et al.[43,44] and Hansis et al.[30] does not enable us to obtain the quantifiable uncertainties for trends.

Apart from the above two bookkeeping approaches, here we developed another way (the third approach to calculate E_{LUC} in this study) to indirectly estimate E_{LUC} using the difference of land carbon flux from atmospheric inversions, the flux from lateral transport and the flux from DGVMs under S2 simulation (driven by rising CO_2 and climate change, not taking into account the lateral transport flux) (E_{ILD}). This approach was based on the assumption that the effect of changing atmospheric CO_2 concentration and climate are well modelled by DGVMs so that the difference between inversion fluxes (including all CO_2 sources and components), lateral carbon flux and DGVM-modelled fluxes under S2 simulation equals the net source from land use and land management.

The processes of lateral carbon transport generally involve (1) the trade of food and wood products; (2) carbon export from land to ocean by rivers. In terms of the lateral carbon flux associated with food and wood trade (Supplementary Fig. 12), we first derive the annual import and export data of food and wood products from FAO statistical databases (http://www.fao.org/faostat/en/#data). Then the food and wood data are converted into dry biomass and into carbon using specific conversion factors. For food products, we adopted crop-specific coefficients (including dry matter content of harvested biomass and carbon content of harvested dry matter; see Supplementary Table 6) following Wolf et al.[45] and Kyle et al.[46]. For wood products, we adopted an average wood density of 0.5 and 0.45 carbon concentration in dry biomass following Ciais et al.[47]. In terms of the carbon exported from ecosystems by rivers, we included dissolved organic carbon, particulate organic carbon and dissolved inorganic carbon from 45 major zones (MARCATS: MARgins and CATchments Segmentation) and 149 subunits (COSCATs: Coastal Segmentation and related CATchments)[48,49] (see Supplementary Table 7). Then we aggregated the riverine carbon transport to the continental scale (Supplementary Fig. 13). However, it should be noted that the carbon transport data are only a rough estimate and lack temporal evolution. Besides, it is unclear whether the exported carbon by rivers is from old deposits or from current photosynthesis. In addition, time series of the carbon exports from rivers are not available. Therefore, we did not count this part in the calculation of the lateral transport flux.

We obtained 16 estimates from the E_{ILD} approach, as eight DGVMs and two atmospheric inversions were considered in the analysis. All datasets from atmospheric inversions and DGVMs were first regridded into a common 0.5° × 0.5° grid using the nearest-neighbour interpolation method. We also performed the same analyses by regridding all the datasets into a common 1° × 1° or 2° × 2° grid, and found similar results (Supplementary Fig. 14). In addition, given that BK was based on national data and not spatially explicit, we obtained latitudinal results (the bottom left panel in Fig. 3) by roughly aggregating northern North America, Europe and Asian Russia into the boreal region, southern North America, West/Central/South Asia and East Asia to the Northern Hemisphere temperate region, South America, Africa and southeast Asia to the tropics, and Oceania to the Southern Hemisphere temperate region.

There is a S3 simulation of TRENDY in which DGVMs are driven by the land cover dataset (Land Use Harmonization) in addition to change in climate and atmospheric CO_2. Thus, the difference of S3 and S2 simulations may also represent the model-simulated emission of land-use change. However, comparing the

differences between S3 and S2 and E_{LUC} estimated by the bookkeeping or inversion-based approach is difficult, because DGVMs do not simulate the full range of processes related to E_{LUC} (not all DGVMs account, for example, for wood and crop harvest or shifting cultivation[42]). Further, land-use change emissions derived from a difference between S3 and S2 differ in the terms that are included as compared to other approaches[50]. Most notably, the loss of additional sink capacity is attributed to E_{LUC} using S3 minus S2, whereas it is excluded from E_{LUC} values derived from bookkeeping models or the inversion-based approach. Lastly, the input land cover dataset has discontinuity issues for the most recent decade and different models also make different assumptions when converting the Land Use Harmonization dataset into model-specific land cover inputs, making it less reliable for estimating trends in the most recent decade. Therefore, we do not include the difference in the S3 and S2 simulations by DGVMs in this study.

Statistical analysis. We calculated the trends of NLS, NPP, HR, NDVI and E_{LUC} during three study periods (1980–2012, 1980–1998, and 1998–2012) based on linear least-squares regression analysis, in which the above five indicators were regarded as dependent variables and year as an independent variable. The slope of the regression was then defined as the trend. The standard error of linear regression coefficient (slope) was defined as the uncertainty of the linear trend. Note that for the average trend of different data sources, the uncertainty of its trend was estimated as the root mean square of the standard error of each data source under the assumption that data from different datasets are independent from each other. Based on this, we obtained the change of above five indicators' trend between the second period (1998–2012) and the first period (1980–1998). The dividing year 1998 is selected according to the Intergovernmental Panel on Climate Change description of the warming hiatus period[16]. However, the intensification of NLS and dominant contribution of E_{LUC} will not change, if trend analyses start from 2001/2002 after the El Niño/La Niña events at the end of the twentieth century (Supplementary Table 2). Note that here changes in the intensity of each component of NLS were indicated by changes in the magnitude (absolute value) of each term. In this case, a positive trend in NPP or HR, F and E_{LUC} refers to an increase of carbon assimilation or carbon emission, and vice versa, a negative trend in NPP or HR, F and E_{LUC} indicates a decline in carbon assimilation or carbon emission. The statistics of the change in trend for each flux were estimated using bootstrap analyses[51]. We first obtained the probability distribution of the NLS trend before and after 1998 in 500-time bootstrapping. Then the probability distribution of the change in trend for each flux was calculated based on the differences of trends among the sampling of the two probability distributions. For clarification, NLS intensification indicates an increase in the trend of NLS after 1998. Similarly, acceleration or deceleration of a flux (NPP, HR, F and E_{LUC}) indicates a larger or smaller trend of the flux during 1998–2012 than that during the 1980s–1998.

Data availability. The GIMMS $NDVI_{3g}$ datasets are available at http://ecocast.arc.nasa.gov/data/pub/gimms/3g.v0/. The satellite-derived NPP dataset is available on request from W. K. Smith[12]. The MODIS NPP dataset is available on request from M. Zhao[5]. The E_{LUC} estimated using the bookkeeping approach is available on request from R. A. Houghton[12] and J. Pongratz[30], respectively. Model outputs generated by DGVM groups are available from S. Stich (s.a.sitch@exeter.ac.uk) or P. Friedlingstein (p.friedlingstein@exeter.ac.uk) upon request.

References

34. Tucker, C. J. et al. An extended AVHRR 8-km NDVI dataset compatible with MODIS and SPOT vegetation NDVI data. *Int. J. Remote Sens.* **26**, 4485–4498 (2005).
35. Keeling, R. F., Piper, S. C., Bollenbacher, A. F. & Walker, J. S. in *Trends: A Compendium of Data on Global Change* (Carbon Dioxide Information Analysis Center, Oak Ridge National Laboratory, US Department of Energy, Oak Ridge, 2009); https://doi.org/10.3334/CDIAC/atg.035
36. Klein Goldewijk, K., Beusen, A., Van Drecht, G. & De Vos, Martine The HYDE 3.1 spatially explicit database of human-induced global land-use change over the past 12,000 years. *Glob. Ecol. Biogeogr.* **20**, 73–86 (2011).
37. Goldewijk, K. A historical land use data set for the Holocene; HYDE 3.2. *EGU General. Assem. Conf. Abstr.* **18**, 1574 (2016).
38. Peylin, P. et al. Global atmospheric carbon budget: results from an ensemble of atmospheric CO_2 inversions. *Biogeosciences* **10**, 6699–6720 (2013).
39. Chevallier, F. et al. CO_2 surface fluxes at grid point scale estimated from a global 21 year reanalysis of atmospheric measurements. *J. Geophys. Res.* **115**, D21307 (2010).
40. Rödenbeck, C. *Estimating CO_2 Sources and Sinks from Atmospheric Mixing Ratio Measurements using a Global Inversion of Atmospheric Transport* Tech. Rep. 6 (Max Planck Institute for Biogeochemistry, Jena, 2005); http://www.bgc-jena.mpg.de/uploads/Publications/TechnicalReports/tech_report6.pdf
41. Thompson, R. L. et al. Top–down assessment of the Asian carbon budget since the mid 1990s. *Nat. Commun.* **7**, 10724 (2016).
42. Le Quéré, C. et al. Global carbon budget 2016. *Earth Syst. Sci. Data* **8**, 605 (2016).
43. Houghton, R. A. et al. Changes in the carbon content of terrestrial biota and soils between 1860 and 1980: a net release of CO_2 to the atmosphere. *Ecol. Monogr.* **53**, 235–262 (1983).
44. Houghton, R. A. Revised estimates of the annual net flux of carbon to the atmosphere from changes in land use and land management 1850–2000. *Tellus B* **55**, 378–390 (2003).
45. Wolf, J. et al. Biogenic carbon fluxes from global agricultural production and consumption. *Glob. Biogeochem. Cycles* **29**, 1617–1639 (2015).
46. Kyle, P. et al. *GCAM 3.0 Agriculture and Land Use: Data Sources and Methods* PNNL-21025 (Pacific Northwest National Laboratory, 2011); https://doi.org/10.2172/1036082
47. Ciais, P. et al. The impact of lateral carbon fluxes on the European carbon balance. *Biogeosci. Discuss.* **3**, 1529–1559 (2006).
48. Laruelle, G. G. et al. Global multi-scale segmentation of continental and coastal waters from the watersheds to the continental margins. *Hydrol. Earth Syst. Sci.* **17**, 2029 (2013).
49. Regnier, P. et al. Anthropogenic perturbation of the carbon fluxes from land to ocean. *Nat. Geosci.* **6**, 597–607 (2013).
50. Pongratz, J., Reick, C. H., Houghton, R. & House, J. Terminology as a key uncertainty in net land use and land cover change carbon flux estimates. *Earth Syst. Dyn.* **5**, 177 (2014).
51. Manly, B. F. J. *Randomization, Bootstrap and Monte Carlo Methods in Biology* (CRC Press, Boca Raton, 2006).